

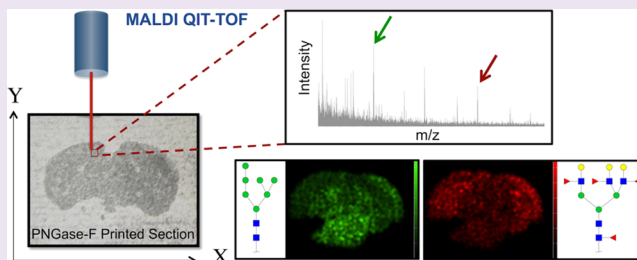
# Imaging of N-Linked Glycans from Formalin-Fixed Paraffin-Embedded Tissue Sections Using MALDI Mass Spectrometry

Shadi Toghi Eshghi,<sup>†</sup> Shuang Yang,<sup>‡</sup> Xiangchun Wang,<sup>‡</sup> Punit Shah,<sup>‡</sup> Xingde Li,<sup>†</sup> and Hui Zhang<sup>\*‡</sup>

<sup>†</sup>Department of Biomedical Engineering, <sup>‡</sup>Department of Pathology, School of Medicine, Johns Hopkins University, Baltimore, Maryland 21231, United States

## S Supporting Information

**ABSTRACT:** Aberrant glycosylation is associated with most of the diseases. Direct imaging and profiling of N-glycans on tissue sections can reveal tissue-specific and/or disease-associated N-glycans, which not only could serve as molecular signatures for diagnosis but also shed light on the functional roles of these biomolecules. Mass spectrometry imaging (MSI) is a powerful tool that has been used to correlate peptides, proteins, lipids, and metabolites with their underlying histopathology in tissue sections. Here, we report an MSI technique for direct analysis of N-glycans from formalin-fixed paraffin-embedded (FFPE) tissues. This technique consists of sectioning FFPE tissues, deparaffinization, and rehydration of the sections, denaturing tissue proteins, releasing N-linked glycans from proteins by printing peptide-N-glycosidase F over the sections, spray-coating the tissue with matrix, and analyzing N-glycans by matrix-assisted laser desorption/ionization mass spectrometry (MALDI-MS). Brain sections from a C57BL/6 mouse were imaged using this technique at a resolution of 100  $\mu\text{m}$ . Forty-two N-glycans were analyzed from the mouse brain section. The mass spectrometry images were used to study the relative abundance of oligomannose, nonfucosylated, and fucosylated complex N-glycans in different brain areas including isocortex, hippocampal formation, and brainstem and specific glycans associated with different areas of the brain were identified. Furthermore, glioblastoma tumor xenografts in a NOD/SCID mouse were imaged. Several glycans with differential expression in tumor versus normal brain tissues were identified. The MSI technique allows for imaging of N-glycans directly from FFPE sections. This method can potentially identify tissue-specific and/or disease-associated glycans coexpressed with other molecular signatures or within certain histological structures.



Glycans coat the surface of all living cells, controlling their interactions with their extracellular environment. They are sugar chains that are post-translationally attached to more than half of the total human proteins and mediate their function.<sup>1</sup> In fact, glycans carry much of the information content of living systems, thus relating the genomics data with the observed phenotype.<sup>2</sup> Glycans play vital roles in almost any biological process, such as cell proliferation, cell–cell and cell–extra cellular matrix interactions, protein degradation, inflammation, and activation of the immune system.<sup>1</sup> They are involved in almost all diseases such as cancer, cardiovascular diseases, neurodegenerative diseases, and disorders of immune system.<sup>3</sup> N-glycans are the subgroup of glycans that comprise of sugar chains that are attached to the asparagine (Asn) residue of the polypeptides in the Asn-X-Ser or Asn-X-Thr sequons, where X can be any amino acid except proline. Imaging of tissue N-glycans is an essential, yet less-explored tool for studying their functions. In contrast to conventional glycan profiling assays, where the tissue is first homogenized, imaging focuses on studying the glycosylation heterogeneity in pathologically or structurally different regions of the tissue. Therefore, it can provide an invaluable means to understanding the roles of N-glycans in the physiology and molecular pathology of the diseases.

Histochemical staining using lectin is by far the most common method for visualization of glycosylation from formalin-fixed paraffin-embedded (FFPE) tissue sections. For instance, Concanavalin A (ConA) and Aleuria Aurantia Lectin (AAL) are two of the lectins that are used in histostaining of oligomannose and fucosylated glycans, respectively.<sup>4</sup> Despite its contributions to the studies on glycosylation in pathological tissue sections, this technique is limited in many ways. First, lectins provide minimal structural information about the stained epitopes. For example, ConA can bind internal and non-reducing terminal  $\alpha$ -mannose,<sup>5</sup> thus staining a variety of oligomannose structures. Therefore, the ConA staining cannot specify the structure of the glycans. In addition, they often fail to differentiate between different glycan subgroups. For instance, AAL can bind the fucose residues on both N-linked and O-linked glycans. Second, due to steric hindrance of different glycan epitopes, lectin histostaining is limited to very few lectins at a time on each tissue section, thus making multiplex glycan imaging very challenging. Third, histostaining

Received: May 22, 2014

Accepted: July 16, 2014

Published: July 16, 2014

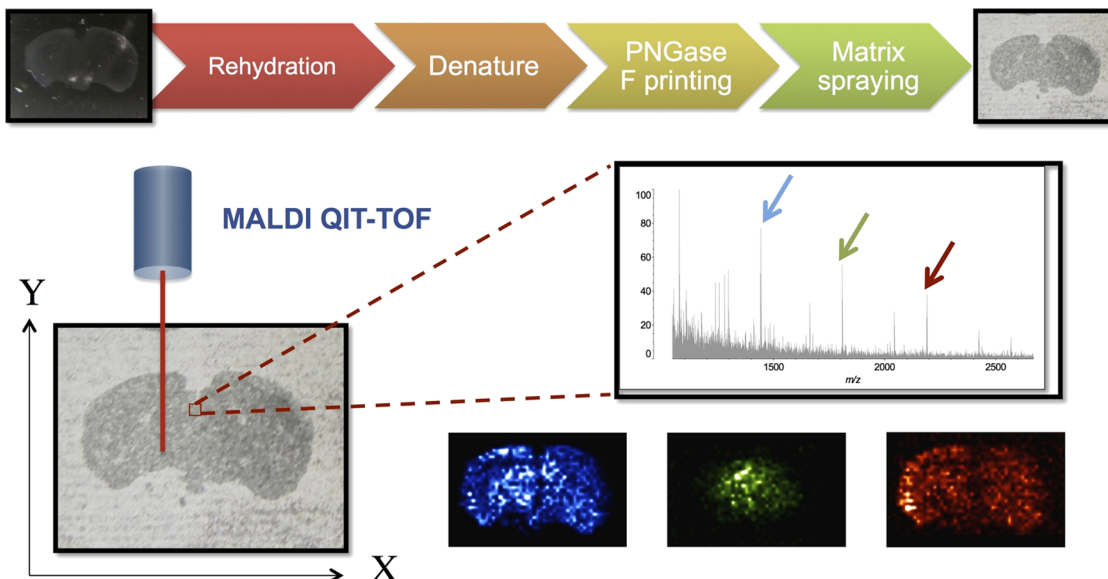


**Figure 1.** Schematic workflow of mass spectrometry imaging of N-linked glycans from FFPE sections. An FFPE tissue section is first deparaffinized and rehydrated. The tissue proteins are denatured by treatment with a basic antigen retrieval buffer and baking in a water bath for 20 min followed by incubation in a 40 mM DTT solution. To preserve the spatial information on the glycans, a microarray printer is used to apply the PNGase F on the tissue in a grid. The section is incubated in a humidity chamber at 37 °C overnight. After air-drying the tissue, DHB matrix is sprayed over the section using an artistic airbrush followed by analyzing by MALDI-MS. The major difference between a conventional MALDI analysis and an imaging experiment is that here, the tissue is raster scanned by the laser in the *x* and *y* directions and mass spectra are acquired for each pixel on the tissue. At this point, by mapping the intensity of various peaks as a function of location, ion images can be generated for each glycan structure detected in the mass spectra. The ion image corresponding to each mass spectral peak from the MALDI-MS spectra is shown in a different color.

methods lack quantification accuracy. Compared to the lectins, glycan antibodies are more specific with respect to the glycan determinants. However, the number of currently developed monoclonal antibodies for glycans is far from covering the width of the mammalian glycans.<sup>2</sup> Therefore, alternative imaging techniques are essential to complement the information acquired from histostaining assays.

Mass spectrometry imaging (MSI) has been previously applied for spatially resolved profiling of proteins, lipids, small molecule metabolites, and drugs from tissue sections.<sup>6–10</sup> Owing to the high sensitivity and specificity of mass spectrometric analysis, MSI has overcome some of the challenges of conventional histostaining techniques. Unlike affinity-based detection methods such as immunohistochemistry staining, where the detection relies on some understanding of the analyte of interest, MSI does not require any *a priori* knowledge of the glycans. This attribute, which is a unique characteristic of MSI, is particularly desirable for discovery research. In addition, hundreds of analytes can be detected and identified from one single mass spectrometry experiment, resulting in high-content molecular profiling with spatial information in tissue sections. Furthermore, MSI can be combined with quantitative and semiquantitative mass spectrometry analysis techniques to facilitate quantitative imaging of different analytes directly from tissue sections. The recent advances in mass spectrometry techniques and data interpretation have significantly pushed the limits of glycomics studies.<sup>11</sup> However, the low ionization efficiency of native glycans compared to other macromolecules such as proteins and lipids makes them challenging to study in complex mixtures. Therefore, glycans are often isolated from extracts of biological samples and chemically modified (e.g., permethylated) before mass spectrometry analysis.<sup>12,13</sup> In this glycomics procedure, the spatial information on glycans is lost due to

homogenization of the sample. Recently, we demonstrated that glycans released from glycoproteins that were immobilized on a solid phase could be directly analyzed by mass spectrometry. This method does not require further purification of glycans to remove interferences from proteins and peptides.<sup>14,15</sup> This attribute is crucial for development of a glycomics study platform for imaging of glycans from samples with the high biological complexity of the tissues.

In this study, we developed a mass spectrometry-based platform for imaging of N-linked glycans from formalin-fixed paraffin-embedded (FFPE) tissue sections. In this technique, FFPE tissue sections are mounted on glass slides, which results in immobilization of the tissue glycoproteins on the slides. N-linked glycans are then selectively released from glycoproteins of tissue section by applying PNGase F enzyme using a microarray printer. The matrix-coated slides are subsequently analyzed by MALDI-MS. The acquired mass spectral images show the distribution of the N-linked glycans over the tissue section. Imaging of the N-linked glycans from FFPE coronal mouse brain tissue sections using this method revealed the spatial distribution of 42 N-linked glycans. In addition, the results showed that N-glycans are present in all regions of the brain. However, certain modifications are more abundant in particular brain structures. For example, brainstem (BS) is richer in oligomannose and nonfucosylated complex N-glycans, while the majority of the fucosylated N-glycans are more abundant in isocortex (IsoCTX) and the hippocampal formation (HPF). These observations were also compared with histostaining of adjacent tissue sections with AAL and ConA lectins. In addition, glioblastoma brain tumor xenografts from a NOD/SCID mouse were imaged by MALDI-MS. Based on the acquired ion images, several N-glycans with differential expression in tumor versus adjacent normal tissues were distinguished, most of which were more abundant in the tumor.

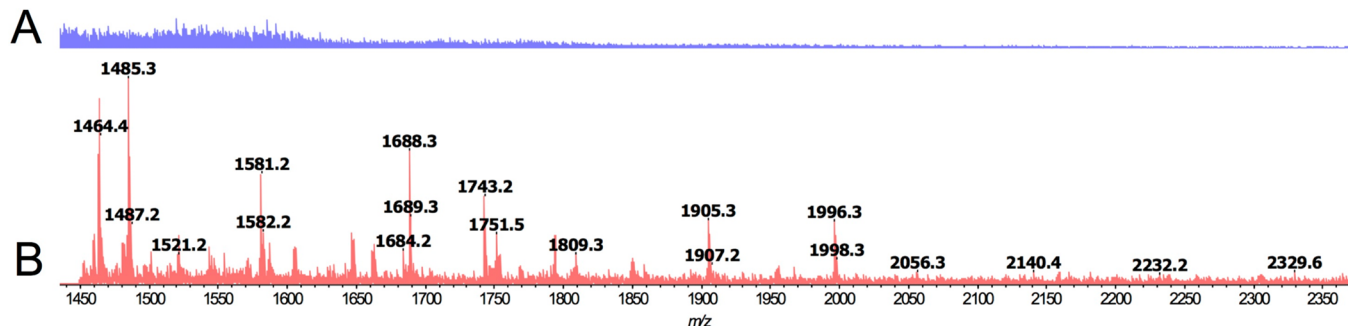


**Figure 2.** Direct analysis of N-glycans released by PNGase F from FFPE tissue section using MALDI-MS. (A) PNGase F negative and (B) PNGase F positive. PNGase F is printed over the mouse brain coronal section at 100  $\mu\text{m}$  spacing. The enzyme is printed on one-half of the tissue section, while the other half is treated with only the buffer. Mass spectra are acquired for a 1  $\text{mm}^2$  area on each brain half using MALDI-MS. The mass spectrum of the PNGase F negative part shows very low signal, while several N-glycan peaks are detected on the PNGase F positive sample.

The N-linked glycan mass spectrometry imaging platform not only helps identify the N-linked glycans directly from FFPE tissue sections but also determines the spatial distribution of unique glycan structures over the tissue. This technique provides complementary information to the traditional histostaining methods, which is essential to fully characterize the functional and pathological roles of N-linked glycosylation in tissues.

## RESULTS AND DISCUSSION

Mass spectrometry imaging of glycans relies on enzymatic release of N-glycans from the proteins that had been immobilized on the glass slide. The attachment of proteins to solid phase minimizes their interference with the glycan mass spectral signal. The glycan imaging consists of multiple steps, including deparaffinizing and rehydrating the FFPE section followed by antigen retrieval to recover the protein reactivity thus improving the efficiency of the PNGase F digestion. After equilibrating the pH of the tissue section followed by air-drying, PNGase F is printed over the section in a grid at a spatial resolution of 100  $\mu\text{m}$  using a microarrayer. The PNGase F-printed tissue is then incubated in a temperature-controlled humidity chamber to complete deglycosylation. The matrix solution is sprayed over it, and the matrix-coated section is imaged by MALDI-MS. Figure 1 shows a representative schematic of the workflow for imaging of N-linked glycans from FFPE tissue sections.

**Direct Analysis of PNGase F-Released N-Glycans from FFPE Tissue Section Using MALDI-MS.** To determine whether glycans could be released and directly analyzed by MALDI-MS from glycoproteins immobilized on conductive slides, mouse brain coronal sections were analyzed. PNGase F was printed over the right half of a section, while buffer was printed over the other half at spacing of 100  $\mu\text{m}$  as a negative control. A 1  $\text{mm}^2$  area of each of the PNGase F negative and positive parts of the brain was imaged using MALDI-MS separately. Figure 2 shows the mass spectra corresponding to the PNGase F-negative (Figure 2A) and PNGase F-positive (Figure 2B) parts of the brain in the mass range 1450–2400 Da. The mass spectral peaks in the bottom panel represent the N-glycans that are released from the glycoproteins in the PNGase F-treated section.

To further ensure that the mass spectral signal corresponds to the glycans, collision-induced dissociation (CID) tandem mass spectrometry (MS/MS) was performed on the mass peaks in the MS1 spectrum. While not all of the mass spectral peaks

were high enough to generate high-quality MS/MS spectra, the majority possessed the glycan signature mass differences of 162.05 and 203.08 corresponding to masses of a hexose (Hex) and N-acetylhexosamine (HexNAc) from N-glycans, respectively. The MS/MS spectra of two selected peaks corresponding to H7N2F0 and H4N4F1 are depicted in Figure 3 and Supporting Information S1. For comparison, glycomics analysis was conducted on mouse brain tissue extracts using glycoprotein immobilization for glycan extraction, which is described in detail previously.<sup>14</sup> The MS/MS spectra for the low-intensity peaks in the MALDI imaging spectra were acquired from the mouse brain extracted glycans to confirm their composition (Supporting Information S1). The fragment ions were manually assigned to the mass spectra with the help of the GlycoWorkbench fragmentation tool.<sup>16</sup>

### Identification of N-Glycans from C57BL/6 Mouse Brain Sections.

Analyzing the tissue section with MALDI-QIT-MS resulted in detection and identification of 42 N-linked glycans (Table 1), where 30 (71.4%) of them were fucosylated and 7 (16.7%) of them were nonfucosylated complex glycans. All of the five oligomannose glycans (Man5, Man6, Man7, Man8, and Man9), constituting the 11.9% of the detected glycans, were identified. A list of the detected glycans is given in Table 1, where each N-glycan is depicted by its number of hexose (H), N-acetylhexosamine (N), and fucose (F) residues. The glycan composition identification was performed by first matching the peak mass with a database of all possible mammalian N-glycan compositions and then refined by comparing the results with the Consortium for Functional Glycomics databases and the literature to remove the biologically irrelevant matches. Last, the glycan composition assignment was confirmed by evaluating the corresponding MS/MS spectra. Fucosylation could happen at the core or at the nonreducing ends of the glycans. Heavier, more branched glycans were generally lower in abundance and harder to detect. The largest identified N-linked glycan was a highly branched structure with  $[\text{M} + \text{Na}]^+$  theoretical mass of 2669.967 Da. In this experiment, however, sialylated glycans were missing from the spectrum. One possible explanation for this observation is the loss of sialic acid residues during mass spectrometry analysis by MALDI.<sup>17,18</sup> The identified glycans were compared with the mouse brain glycans reported on the Consortium for Functional Glycomics (CFG) database (<http://www.functionalglycomics.org>). The CFG database contains 31 unique nonsialylated N-glycan peaks in wild type C57BL/6 mouse brain tissue, 27 (87.1%) of which were detected in this

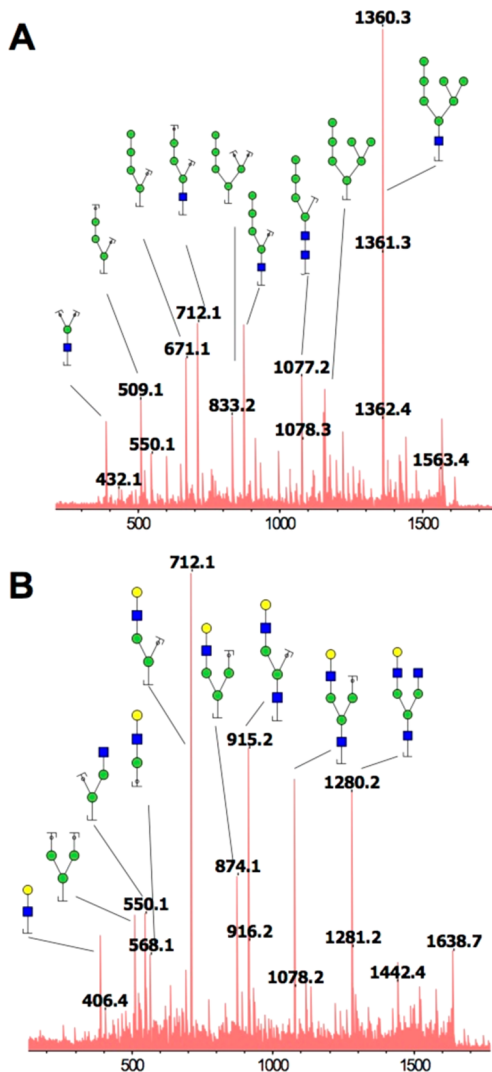


**Figure 3.** Examples of CID MS/MS spectra of the detected glycan peaks. (A) H7N2F0 and (B) H4N4F1. Mass differences of 162.05 and 203.08 in MS/MS spectra are characteristic of glycans, which occur due to loss of Hex and HexNAc. The fragment ions are assigned to the mass spectra using the GlycoWorkbench tool. The acquired MS/MS spectra further support the specificity of this imaging technique to N-glycans.

experiment. These 27 glycan peaks are marked with a tick on the “previously reported” column in Table 1. From the 15 N-glycan peaks that were identified in this study but not listed on the CFG data, 5 N-glycan peaks were identical to the desialylated counterparts of sialylated N-glycans in CFG mouse brain database. These 5 N-glycan peaks are marked with a cross on the “previously reported” column in Table 1. The remaining 10 N-glycan masses had been previously reported in human plasma and serum samples,<sup>19,20</sup> 4 of which had also been detected in mouse brain tissue in a study conducted by Hu et al.<sup>21</sup> or in whole rat brain tissue in another study conducted by Chen et al.<sup>22</sup> These 10 glycan peaks are marked by a plus sign on the “previously reported” column in Table 1. This observation further supports that N-glycans can be directly released and identified from glycoproteins immobilized on slides. However, unprotected sialic acid residues have been lost during the acquisition of the mass spectra using MALDI.<sup>17,18</sup>

**Imaging of N-Glycans in Different Regions of Mouse Brain Sections.** The ion images corresponding to 5 representative fucosylated N-glycans, H4N4F2, H5N4F3, H5NSF2, H4N6F2, and H6NSF4 are presented in Figure 4B–F. The signal intensity for each ion image is obtained by dividing the peak area of each glycan to the normalized peak area of the internal glycan standard (DP7) that had been spiked in PNGase F digestion solution during printing. In this study, we have divided the brain into three major regions of brainstem (BS), isocortex (IsoCTX), and hippocampal formation (HPF). The AAL lectin histostaining of an adjacent mouse brain section is shown in Figure 4A. AAL preferentially binds to fucose ( $\alpha$ -1,6) or ( $\alpha$ -1,3) linked to N-acetylhexosamine. The AAL staining as well as the ion images indicate that fucosylation occurs in all regions of the brain; however, its prevalence seems to depend on the region. The AAL staining is strongest in the IsoCTX followed by HPF and generates the weakest signal in the BS (Figure 4A). Thirty fucosylated N-glycans are identified in this study, which comprises more than 70% of total number of glycans. This diversity in the number of the fucosylated N-glycans is also observed in their spatial distribution. While some of the fucosylated N-glycans such as H4N6F2 (Figure 4E) are more abundant in the BS, the majority of them show a stronger presence in the IsoCTX and HPF. In summary, the fucosylation increases from the center of the brain toward the cortex. One crucial fact in comparing the lectin histostaining data with the MSI images is that the specificity of the lectins is far lower than the mass spectrometry. In fact, AAL staining depicts a superposition of all the ( $\alpha$ -1,6) or ( $\alpha$ -1,3) linked fucose-containing N- or O-linked glycans. Therefore, even though similar patterns between the two are expected, lectin histostaining results are not necessarily reflective of the distribution of single N-glycans over the tissue, which explains the differences observed between the lectin staining and MSI results for each individual glycan.

The ion images corresponding to 5 oligomannose structures of Man5 (HSN2F0), Man6 (H6N2F0), Man7 (H7N2F0), Man8 (H8N2F0), and Man9 (H9N2F0) are depicted in Supporting Information Figure S1. The ConA lectin histostaining of an adjacent section is depicted in Supporting Information Figure S1-A. ConA binds the  $\alpha$ -mannose residues attached to the glycans. Therefore, both the oligomannose and hybrid N-glycans are potential targets for ConA. The ConA staining shows that terminal  $\alpha$ -mannose residues are present in all of the aforementioned regions; however, the signal is stronger in the IsoCTX and BS compared to the HPF (Supporting Information Figure S1-A). The ion images also confirm that oligomannose N-glycans are more abundant in the BS. The ConA staining shows a slight asymmetry between the left and right half of the brain, particularly in the IsoCTX area. This asymmetry, which could be due to the tissue sectioning, was also observed on the ion images of oligomannose N-glycans. Two additional adjacent tissue sections were similarly analyzed to ensure the reproducibility of the results.

**Imaging of N-Glycans in Glioblastoma Tumor Implanted in NOD/SCID Mouse Brain.** Analysis of the tumor implanted mouse brain sections confirmed that glycosylation is altered during tumorigenesis. Mass spectrometry imaging of these sections revealed 13 N-glycans with different expression levels in the tumor compared to the normal brain tissue. These N-glycans are listed in Table 2. To identify these glycans, two regions of interest (ROI) are defined in the brain, such that one ROI surrounds the tumor site and

**Table 1. Detected N-Glycans from Mass Spectrometry Imaging of Mouse Brain Sections<sup>a</sup>**

no.	symbol	Hex (H)	HexNAc (N)	Fuc (F)	theoretical mass [M + Na] <sup>+</sup>	detected mass [M + Na] <sup>+</sup>	previously reported	in situ MS/MS identification
1	H5N2F0	5	2	0	1257.4231	1257.343	✓	yes
2	H3N3F1	3	3	1	1282.4548	1282.368	+	yes
3	H4N3F0	4	3	0	1298.4497	1298.387	+	yes
4	H3N4F0	3	4	0	1339.4763	1339.417	+	yes
5	H5N2F1	5	2	1	1403.4810	1403.429	+	yes
6	H6N2F0	6	2	0	1419.4759	1419.405	✓	yes
7	H4N3F1	4	3	1	1444.5076	1444.413	+	yes
8	H5N3F0	5	3	0	1460.5025	1460.401	+	yes
9	H3N4F1	3	4	1	1485.5342	1485.456	✓	yes
10	H4N4F0	4	4	0	1501.5291	1501.446	+	yes
11	H3NSF0	3	5	0	1542.5557	1542.473	+	yes
12	H7N2F0	7	2	0	1581.5287	1581.446	✓	yes
13	H5N3F1	5	3	1	1606.5604	1606.455	✓	yes
14	H4N4F1	4	4	1	1647.5870	1647.482	✓	yes
15	H5N4F0	5	4	0	1663.5819	1663.476	✓	yes
16	H3NSF1	3	5	1	1688.6136	1688.508	✓	yes
17	H8N2F0	8	2	0	1743.5815	1743.498	✓	yes
18	H6N3F1	6	3	1	1768.6132	1768.494	✓	no
19	H4N4F2	4	4	2	1793.6449	1793.523	✓	yes
20	H5N4F1	5	4	1	1809.6398	1809.524	✓	yes
21	H4NSF1	4	5	1	1850.6664	1850.579	✓	yes
22	H9N2F0	9	2	0	1905.6343	1905.517	✓	yes
23	H5N4F2	5	4	2	1955.6977	1955.562	✓	yes
24	H6N4F1	6	4	1	1971.6926	1971.554	✓	no
25	H4NSF2	4	5	2	1996.7243	1996.588	✓	yes
26	H5NSF1	5	5	1	2012.7192	2012.541	✓	yes
27	H4N6F1	4	6	1	2053.7458	2053.533	✗	no
28	H5N4F3	5	4	3	2101.7556	2101.571	✓	no
29	H6N4F2	6	4	2	2117.7505	2117.567	✓	no
30	H5NSF2	5	5	2	2158.7771	2158.541	✓	no
31	H6NSF1	6	5	1	2174.7720	2174.591	+	no
32	H4N6F2	4	6	2	2199.8037	2199.585	✓	no
33	H5N6F1	5	6	1	2215.7986	2215.570	✗	no
34	H6N6F0	6	6	0	2231.7935	2231.558	+	no
35	H5NSF3	5	5	3	2304.8350	2304.575	✓	no
36	H6NSF2	6	5	2	2320.8299	2320.604	✗	no
37	H5N6F2	5	6	2	2361.8565	2361.589	✓	no
38	H6NSF3	6	5	3	2466.8878	2466.621	✓	no
39	H5N6F3	5	6	3	2507.9144	2507.661	✓	yes
40	H6N6F2	6	6	2	2523.9093	2523.572	✗	no
41	H6NSF4	6	5	4	2612.9457	2613.742	✓	no
42	H6N6F3	6	6	3	2669.9672	2670.694	✗	no

<sup>a</sup>Each glycan in the table is shown by its number of the hexose (Hex or H), N-acetylhexosamine (HexNAc or N) and fucose (Fuc or F) residues. Among the 42 detected N-glycans, 27 had been reported in the CFG database of wild type mouse brain previously (<http://www.functionalglycomics.org>). Of the remaining 15 N-glycans, 5 most likely belong to sialylated glycans reported in the CFG mouse brain database that lost their sialic acid residues during sample preparation or ionization of the analytes. These 5 glycans are marked by a cross on the last column. With the exception of these 5 glycans, all of the remaining 10 detected N-glycans had been reported in human plasma and serum samples in earlier studies.<sup>19,20</sup> Four of these 10 remaining glycans had also been reported in other mouse and rat brain tissue.<sup>21,22</sup>

the other is mirrored in the normal half of the mouse brain. Two-sample *t* test is applied to the signal intensities in the ROIs and a p-value threshold of 0.001 is used to determine which glycans differ in the tumor. Of the 13 altered N-glycans, 10 are increased in the tumor. While there is no obvious glycan structural pattern similarity between the glycans with altered abundances, the less abundant glycans are more fucosylated. For instance, the majority of the nonfucosylated N-glycans such as oligomannose and nonfucosylated complex structures are more abundant in the tumor. Although few fucosylated N-glycans are altered in the tumor cells to draw a general

conclusion, this observation suggests that highly fucosylated glycans carrying antennary fucose residues might be down-regulated in tumor cells. Ion images corresponding to some of these glycans are depicted in Figure 5 as examples. The reproducibility of the results was confirmed by imaging an adjacent tissue section using MSI (Supporting Information Figure S2).

In this study, we have reported an MSI based technique for imaging of N-linked glycans released from immobilized glycoproteins on FFPE sections and demonstrated the application of this technique with two examples. We studied

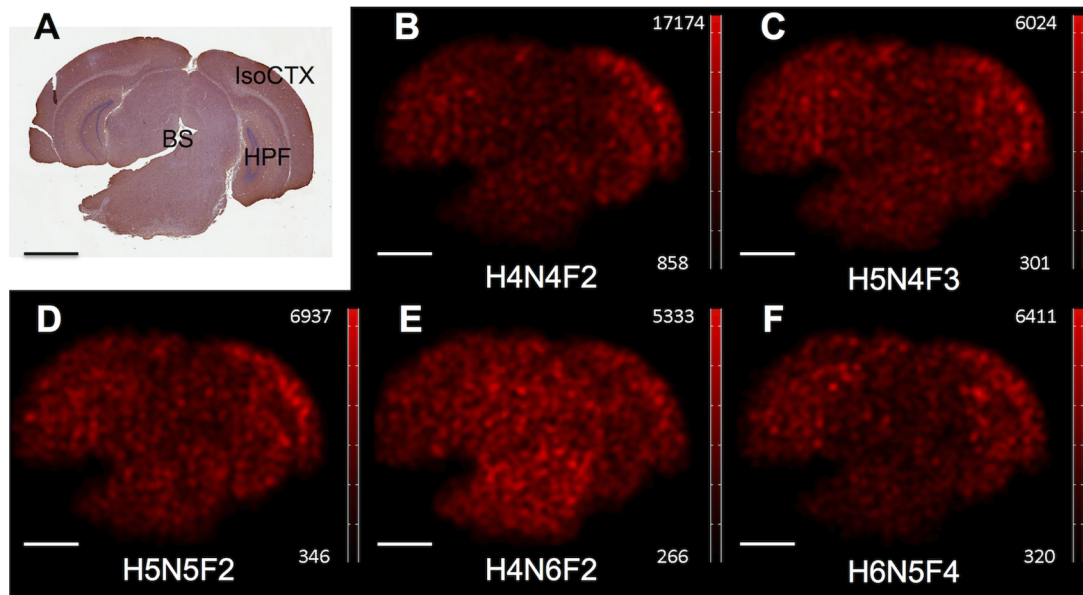


**Figure 4.** Ion images of representative fucosylated glycans along with AAL staining of an adjacent tissue section. (A) Based on the AAL histostaining, fucosylation occurs in all regions of the brain, with a relatively higher abundance in the IsoCTX compared to the HPF, while BS has the lowest abundance of fucosylation. The ion images correspond to the peaks detected at (B) 1793.523 (H4N4F2), (C) 2101.571 (HSN4F3), (D) 2158.541 (HSN5F2), (E) 2199.585 (H4N6F2), and (F) 2613.742 (H6NSF4) Da. The signal intensity in each ion image is calculated by dividing the area of the corresponding peak by the normalized peak area of the internal glycan standard. Scale bar, 2 mm.

**Table 2. N-Glycans and Their Relative Abundance in Tumor versus the Surrounding Normal Brain Tissue<sup>a</sup>**

no.	symbol	no. of Fuc residues	theoretical mass [M + Na] <sup>+</sup>	abundance in tumor
1	H4N3F0	0	1298.4497	higher
2	H6N2F0	0	1419.4759	higher
3	H4N3F1	1	1444.5076	higher
4	H5N3F0	0	1460.5025	higher
5	H7N2F0	0	1581.5287	higher
6	H5N4F0	0	1663.5819	higher
7	H3N5F1	1	1688.6136	lower
8	H8N2F0	0	1743.5815	higher
9	H4N4F2	2	1793.6449	lower
10	H5N4F1	1	1809.6398	higher
11	H9N2F0	0	1905.6343	higher
12	H6N4F1	1	1971.6926	higher
13	H4NSF2	2	1996.7243	lower

<sup>a</sup>Thirteen N-glycans with differential expression in the tumor were identified, most of which were more abundant in the tumor cells. N-glycans that are less abundant in tumor have higher levels of fucosylation.

the spatial distribution of 42 N-glycans on mouse brain coronal sections and also imaged distinct N-glycans in patient-derived glioblastoma tumor cells implanted in a mouse brain. Similar techniques have been developed for direct profiling of tissue glycans such as on-surface enzymatic digestion of N-glycans followed by liquid chromatography–mass spectrometry.<sup>21</sup> However, this method does not preserve the spatial information concerning the distribution of different N-glycans. The developed MSI-based method provides a unique tool for high-throughput imaging of N-glycans from FFPE tissue sections, which distinguishes it from more conventional histostaining methods. It provides unique information regarding the spatial distribution of specific glycan structures over the tissue. This information, combined with histology, can provide potentially invaluable insight into the histopathology of many diseases. The acquired images from the C57BL/6 mouse brain sections suggested that the level of glycosylation and the type of N-glycans varies in different brain structures. Fucosylation was predominantly observed in the brain, such that more than 70% of all the identified glycans appeared to be fucosylated. The most prominent difference in brain N-glycan structures was observed between cerebral cortex and brainstem. While

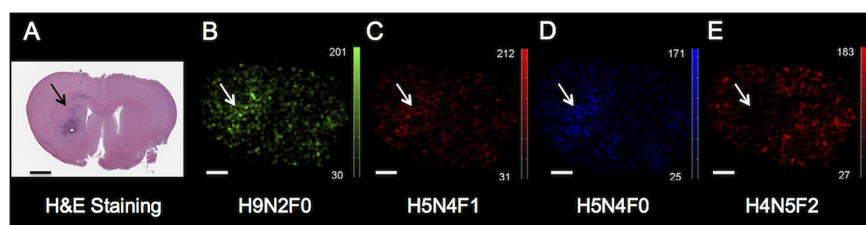


**Figure 5.** Ion images of tumor N-glycans along with H&E staining of an adjacent tissue section. (A) Tumor cells are concentrated around the injection site. The ion images correspond to the peaks detected at (B) 1905.634 (H9N2F0), (C) 1809.640 (HSN4F1), (D) 1663.582 (HSN4F0), and (E) 1996.724 (H4N5F2) Da. The majority of the glycans are more abundant in the tumor; however, a few highly fucosylated glycan peaks are more abundant in the surrounding normal tissues. Scale bar, 1 mm.

oligomannose and nonfucosylated complex structures were more abundant in the brainstem, fucosylated N-glycans showed overall higher signal in the cortex. Our results in the mice brain tumor model showed considerable differences between the N-glycosylation in tumor versus adjacent normal tissues. Low-abundance N-glycans in the tumor cells had higher levels of fucosylation. On the other hand, high-abundance N-glycans in the tumor cells mostly consisted of oligomannose and nonfucosylated complex glycans. Knowing the spatial distribution of N-glycans in different brain structures or pathologies can shed light on the roles that glycosylation plays in mediating the brain functions.

In addition to FFPE sections, frozen tissue sections can also be analyzed by MALDI imaging. In fact, during the preparation of this manuscript, Powers et al. reported imaging of N-linked glycans from frozen tissue sections using MALDI mass spectrometry.<sup>23</sup> For more elaborate results, the current imaging method can be combined with quantitative techniques using isotopic labeled standards for high accuracy quantitation. For example, by spiking in standard glycans labeled with stable isotope tags, one can relatively quantify the images acquired from the tissue sections for targeted glycans.<sup>24,25</sup> In this study, we used the robotic application of the enzyme using the microarray printer with 100  $\mu\text{m}$  spot-to-spot spatial resolution and the mass spectral images were acquired with spatial resolution of 100  $\mu\text{m}$ . High-density deposition of enzyme, high resolution MS acquisition using a faster instrument with higher laser repetition rate<sup>26</sup> and imaging in the microscope mode using a triple focus time-of-flight mass spectrometer<sup>27</sup> could be used to increase the imaging spatial resolution. One of the other important limitations of MALDI-MS imaging is the complexity of the sample preparation. The dependency of the final results on the changes in the sample preparation makes the reproducibility challenging. Incorporation of automatic and semiautomatic sample handling can improve the reproducibility.<sup>28–31</sup>

## METHODS

**Materials and Reagents.** Antigen retrieval buffer was purchased from R&D Systems. Peptide-N-Glycosidase F (PNGase F) was from New England Biolabs, dithiothreitol (DTT), maltoheptaose (DP7), 2,5-dihydroxybenzoic acid (DHB), and *N,N*-Dimethylaniline (DMA) were purchased from Sigma-Aldrich. Biotinylated AAL and ConA lectins and the ABC-Elite kit were from Vector Laboratories. Peroxidase blocking reagent was from Dako.

**Animal Methods.** A male C57BL/6 mouse from Jackson Laboratory was used for this study. It was housed in an animal facility with access to water, food, and libitum. The mouse was euthanized at 20 weeks of age by harvesting organs and tissues: heart, aorta, kidney, liver, brain, and spleen, under anesthesia with Ketamine/Xylazine (100 mg/10 mg per kg IP). For imaging of the mouse brain tumor using MALDI mass spectrometry, 10<sup>6</sup> primary human glioblastoma cells (NS276) were stereotactically injected into the right striatum of an 8-week old, NOD/SCID male mouse (Charles River Laboratories) as previously described.<sup>32</sup> Four weeks following the tumor implantation, the mouse was sacrificed and the brain was extracted. These experiments were approved by the Johns Hopkins University Institutional Animal Care and Use Committee (Protocol numbers MO11M492 and MO12M195).

**Mouse Brain Tissue Fixation and Embedding.** The mouse brain tissues were fixed in 10% (v/v) formalin for 48 h after dissection. Following dehydration, the fixed brain tissues were embedded in paraffin. The samples were sectioned at thickness of 5  $\mu\text{m}$ . The normal brain tissue sections were mounted on indium tin oxide (ITO) coated glass slides (Delta's Technologies), while the tumor brain sections

were mounted on positively charged glass slides. The slides were stored at RT for a maximum of one month until use.

**Tissue Preparation.** The FFPE tissue sections were deparaffinized by three xylene washes, 15 min each. Subsequently, they were rehydrated in graded ethanol solutions of 100, 95, 70, and 50% (v/v). To denature proteins on tissue slides, antigen retrieval procedure was performed by baking the tissue sections in the basic antigen retrieval buffer, pH 9.0 (R&D Systems) for 20 min. This was followed by protein denaturing in 40 mM DTT buffer and steaming for 10 min. Pretreatment of the tissue with denaturing reagents improves the deglycosylation significantly. The tissue was then briefly washed with 1% (v/v) formic acid, 1 M sodium chloride and deionized water. The tissue was further washed with 15 mM ammonium bicarbonate buffer (pH ~ 8.0) for 20 min to equilibrate the pH of the section before applying the PNGase F enzyme.

**Deglycosylation and Matrix Deposition.** PNGase F is the enzyme that cleaves the N-linked glycans from the attached proteins and peptides. A solution of 1 M ammonium bicarbonate buffer was added to PNGase F to bring the final pH to 8, close to the optimal pH for deglycosylation by PNGase F. A solution of 1 mM DP7 was spiked into the enzyme solution as an internal standard to obtain a final concentration of 70 mM. PNGase F mixture was printed over the tissue section using an automated microarrayer (BioRobotics MicroGrid, Isogen Life Science) at 100  $\mu\text{m}$  spacing. The robotic application of the enzyme using the microarray printer not only creates a uniform array of localized enzyme over the tissue but also requires significantly less amount of PNGase F. The PNGase F-printed tissue section was incubated in a humidity chamber (maximum humidity of 80%) at 37 °C overnight. The matrix was prepared by dissolving 120 mg of DHB into 1 mL of 50% (v/v) acetonitrile, 0.1 mM sodium chloride followed by addition of 20  $\mu\text{L}$  of DMA. The matrix solution was uniformly sprayed over the sample using an artistic airbrush (Aztek 470, Testors) according to the method previously described.<sup>33</sup>

**MALDI Imaging.** After the sample was air-dried, it was analyzed by a MALDI-QIT-TOF mass spectrometer (AXIMA Resonance, Shimadzu). The Launchpad software was used to specify the mass analysis parameters such as the mass range, the laser intensity, scanning area, and the spatial resolution. The mass spectral images were acquired in positive mode with 20 shots per profile at laser intensity of 130 in the mass range greater than 1170 Da, by scanning the laser at a spatial resolution of 100  $\mu\text{m}$ . The image resolution was constrained by the acquisition time. At this resolution and with the specified settings, it took about 11 h to image every  $\text{cm}^2$  area of the section. The raw data files were converted to imaging files (.img) using the Launchpad software and the images were visualized and analyzed in MATLAB (R2013b, Mathworks).

**Lectin Histostaining.** Followed by deparaffinization in three xylene washes and rehydration in graded ethanol, the endogenous peroxidase activity was blocked. The lectin (AAL or ConA) was diluted to a final concentration of 20  $\mu\text{g mL}^{-1}$  in Dulbecco's phosphate buffered saline (DPBS) and incubated with the tissue for 30 min at RT. ABC-Elite kit was used for detection of the biotinylated lectin according to the instructions. Diaminobenzidine was applied as the chromogen to visualize the tagged glycans. The tissue was then counterstained with hematoxylin and coverslipped.

## ASSOCIATED CONTENT

### Supporting Information

This material is available free of charge via the Internet at <http://pubs.acs.org>.

## AUTHOR INFORMATION

### Corresponding Author

\*Email: hzhang32@jhu.edu.

### Notes

The authors declare no competing financial interest.

## ACKNOWLEDGMENTS

We thank Dr. S. Chatterjee and D. Bedja from Johns Hopkins School of Medicine for providing the mouse brain samples, Dr. Quinones-Hinojosa and C. Kut from Johns Hopkins School of Medicine for providing the mouse brain tumor samples, and B. Feild for providing technical help with the Shimadzu Axima Resonance. This work was supported in part by the National Institutes of Health under grants and contracts of National Cancer Institute, Clinical Proteomics Tumor Analysis Consortium (U24CA160036), the Early Detection Research Network (EDRN, U01CA152813 and U24CA115102), and R01CA112314; National Heart Lung Blood Institute, Programs Excellence in Glycosciences (P01HL107153), NHLBI Proteomic Center (N01-HV-00240).

## REFERENCES

- (1) Hart, G. W., and Copeland, R. J. (2010) Glycomics hits the big time. *Cell* **143**, 672–6.
- (2) Walt, D., Aoki-Kinoshita, K. F., Bertozzi, C., Boons, G.-J., Darvill, A., Hart, G., Kiessling, L., Lowe, J., Moon, R. J., Paulson, J. C., Sasisekharan, R., Varki, A. P., and Wong, C.-H. (2012) *Transforming Glycoscience: A Roadmap for the Future*; The National Academies Press, Washington, DC.
- (3) Varki, A., Cummings, A. J., Esko, J. D., Freeze, H. H., Stanley, P., Bertozzi, C. R., Hart, G. W., and Etzler, M. E. (2009) Essentials of glycobiology. *Trends Cell Biol.* (Varki, A., Cummings, R. D., Esko, J. D., Freeze, H. H., Stanley, P., Bertozzi, C. R., Hart, G. W., and Etzler, M. E., Eds.), p 752, Cold Spring Harbor Laboratory Press, New York.
- (4) Sharon, N., and Lis, H. (2003) *Lectins*, 2nd ed., Springer, Dordrecht.
- (5) Debray, H., Decout, D., Strecker, G., Spik, G., and Montreuil, J. (1981) Specificity of twelve lectins towards oligosaccharides and glycopeptides related to N-glycosylproteins. *Fed. Eur. Biochem. Soc. J.* **117**, 41–55.
- (6) Stoeckli, M., Chaurand, P., Hallahan, D. E., and Caprioli, R. M. (2001) Imaging mass spectrometry: A new technology for the analysis of protein expression in mammalian tissues. *Nat. Med.* **7**, 493–6.
- (7) Seeley, E. H., Oppenheimer, S. R., Mi, D., Chaurand, P., and Caprioli, R. M. (2008) Enhancement of protein sensitivity for MALDI imaging mass spectrometry after chemical treatment of tissue sections. *J. Am. Soc. Mass Spectrom.* **19**, 1069–77.
- (8) Goto-Inoue, N., Hayasaka, T., Zaima, N., and Setou, M. (2011) Imaging mass spectrometry for lipidomics. *Biochim. Biophys. Acta* **1811**, 961–9.
- (9) Cornett, D. S., Frappier, S. L., and Caprioli, R. M. (2008) MALDI-FTICR imaging mass spectrometry of drugs and metabolites in tissue. *Anal. Chem.* **80**, 5648–53.
- (10) Groseclose, M. R., Massion, P. P., Chaurand, P., and Caprioli, R. M. (2008) High-throughput proteomic analysis of formalin-fixed paraffin-embedded tissue microarrays using MALDI imaging mass spectrometry. *Proteomics* **8**, 3715–24.
- (11) Zaia, J. (2008) Mass spectrometry and the emerging field of glycomics. *Chem. Biol.* **15**, 881–92.
- (12) Dell, a, Reason, a J., Khoo, K. H., Panico, M., McDowell, R. a, and Morris, H. R. (1994) Mass spectrometry of carbohydrate-containing biopolymers. *Methods Enzymol.* **230**, 108–32.
- (13) Zaia, J. (2004) Mass spectrometry of oligosaccharides. *Mass Spectrom. Rev.* **23**, 161–227.
- (14) Yang, S., Li, Y., Shah, P., and Zhang, H. (2013) Glycomic analysis using glycoprotein immobilization for glycan extraction. *Anal. Chem.* **85**, 5555–61.
- (15) Yang, S., Eshghi, S. T., and Chiu, H. (2013) Glycomic analysis by glycoprotein immobilization for glycan extraction and liquid chromatography on microfluidic chip. *Anal. Chem.* **85**, 10117–10125.
- (16) Ceroni, A., Maass, K., and Geyer, H. (2008) GlycoWorkbench: A tool for the computer-assisted annotation of mass spectra of glycans. *J. Proteome Res.* **7**, 1650–1659.
- (17) Harvey, D. J. (1999) Matrix-assisted laser desorption/ionization mass spectrometry of carbohydrates. *Mass Spectrom. Rev.* **18**, 349–450.
- (18) Wheeler, S. F., Domann, P., and Harvey, D. J. (2009) Derivatization of sialic acids for stabilization in matrix-assisted laser desorption/ionization mass spectrometry and concomitant differentiation of  $\alpha(2 \rightarrow 3)$ - and  $\alpha(2 \rightarrow 6)$ -isomers. *Rapid Commun. Mass Spectrom.* **23**, 303–312.
- (19) Stumpo, K. A., and Reinhold, V. N. (2010) The N-glycome of human plasma. *J. Proteome Res.* **9**, 4823–4830.
- (20) Aldredge, D., An, H. J., Tang, N., Waddell, K., and Lebrilla, C. B. (2012) Annotation of a serum N-glycan library for rapid identification of structures. *J. Proteome Res.* **11**, 1958–68.
- (21) Hu, Y., Zhou, S., Khalil, S. I., Renteria, C. L., and Mechref, Y. (2013) Glycomic profiling of tissue sections by LC-MS. *Anal. Chem.* **85**, 4074–4079.
- (22) Chen, Y. J., Wing, D. R., Guile, G. R., Dwek, R. a, Harvey, D. J., and Zamze, S. (1998) Neutral N-glycans in adult rat brain tissue—Complete characterisation reveals fucosylated hybrid and complex structures. *Eur. J. Biochem.* **251**, 691–703.
- (23) Powers, T., and Jones, E. (2013) Matrix assisted laser desorption ionization imaging mass spectrometry workflow for spatial profiling analysis of N-linked glycan expression in tissues. *Anal. Chem.* **85**, 9799–9806.
- (24) Toghi Eshghi, S., Li, X., and Zhang, H. (2012) Targeted analyte detection by standard addition improves detection limits in matrix-assisted laser desorption/ionization mass spectrometry. *Anal. Chem.* **84**, 7626–32.
- (25) Shah, P., Yang, S., Sun, S., Aiyetan, P., Yarema, K. J., and Zhang, H. (2013) Mass spectrometric analysis of sialylated glycans with use of solid-phase labeling of sialic acids. *Anal. Chem.* **85**, 3606–13.
- (26) Spraggins, J. M., and Caprioli, R. M. (2011) High-speed MALDI-TOF imaging mass spectrometry: Rapid ion image acquisition and considerations for next generation instrumentation. *J. Am. Soc. Mass Spectrom.* **22**, 1022–31.
- (27) Klerk, L. a, Altelaar, a. F. M., Froesch, M., McDonnell, L. a, and Heeren, R. M. a. (2009) Fast and automated large-area imaging MALDI mass spectrometry in microprobe and microscope mode. *Int. J. Mass Spectrom.* **285**, 19–25.
- (28) Aerni, H.-R., Cornett, D. S., and Caprioli, R. M. (2006) Automated acoustic matrix deposition for MALDI sample preparation. *Anal. Chem.* **78**, 827–34.
- (29) Baluya, D. L., Garrett, T. J., and Yost, R. a. (2007) Automated MALDI matrix deposition method with inkjet printing for imaging mass spectrometry. *Anal. Chem.* **79**, 6862–7.
- (30) Franck, J., Arafah, K., Barnes, A., Wisztorski, M., Salzet, M., and Fournier, I. (2009) Improving tissue preparation for matrix-assisted laser desorption ionization mass spectrometry imaging. Part 1: Using microspotting. *Anal. Chem.* **81**, 8193–202.
- (31) McDonnell, L. a, van Remoortere, A., van Zeijl, R. J. M., Dalebout, H., Bladergroen, M. R., and Deelder, A. M. (2010) Automated imaging MS: Toward high throughput imaging mass spectrometry. *J. Proteomics* **73**, 1279–82.
- (32) Chaichana, K. L., Guerrero-cazares, H., Capilla-gonzalez, V., Zamora-berridi, G., Achanta, P., Gonzalez-perez, O., Jallo, G. I., Garcia-verdugo, J. M., and Qui, A. (2009) Intra-operatively obtained human tissue: Protocols and techniques for the study of neural stem cells. *J. Neurosci. Methods* **180**, 116–125.
- (33) Garrett, T. J., Prieto-Conaway, M. C., Kovtoun, V., Bui, H., Izgarian, N., Stafford, G., and Yost, R. a. (2007) Imaging of small molecules in tissue sections with a new intermediate-pressure MALDI linear ion trap mass spectrometer. *Int. J. Mass Spectrom.* **260**, 166–176.